Current transport and electronic states in *a,b*-axis-oriented $YBa_2Cu_3O_7/PrBa_2Cu_3O_7/YBa_2Cu_3O_7$ sandwich-type junctions

J. Yoshida, T. Nagano, and T. Hashimoto
Advanced Research Laboratory, Toshiba Corporation, 1, Komukai Toshibacho, Saiwaiku, Kawasaki 210, Japan
(Received 28 September 1995)

Precise measurement of the temperature and voltage dependence of junction conductance has been carried out for *a,b*-axis-oriented $YBa_2Cu_3O_7/PrBa_2Cu_3O_7/YBa_2Cu_3O_7$ sandwich-type junctions to investigate the possible origin of Josephson coupling in these junctions. Regardless of the presence or absence of the Josephson effect, most of the junctions exhibited a dip in conductance around zero voltage in their dI/dV profiles at low temperatures. This dI/dV anomaly was attributed to the existence of a minimum in the density of states due to electron-electron interaction in disordered metals in the vicinity of a tunneling barrier within the junctions. The complex temperature dependence of junction conductance was reproduced well by a theoretical model in which both tunneling conduction paths and variable range hopping paths were assumed to exist within the $PrBa_2Cu_3O_7$ barrier layer. No definite evidence of current transport through a small number of localized levels or a metallic conduction path in $PrBa_2Cu_3O_7$ has been confirmed, even for junctions with a 20-nm-thick barrier layer.

I. INTRODUCTION

The absence of superconductivity in $PrBa_2Cu_3O_7$ (PBCO) makes the material an attractive candidate for an artificial barrier in Josephson junctions with $YBa_2Cu_3O_7$ (YBCO) superconductive electrodes. The possibility of Josephson coupling between two YBCO electrodes through a thick PBCO barrier was first reported by Barner *et al.*[1] Subsequent research carried by Hashimoto *et al.* demonstrated clear evidence of the Josephson effects, including a nearly ideal Fraunhofer-pattern dependence of the critical current, in *a*-axis-oriented YBCO/PBCO/YBCO sandwich-type junctions with a PBCO barrier layer up to 100 nm thickness.[2] Although their junction characteristics were in good accordance with a superconductor–normal metal–superconductor (SNS) weak link in the dirty limit, the coherence length in the PBCO barrier derived from the experimental results was anomalously long, even when the experimentally observed low resistivity of the barrier layer compared to bulk PBCO was regarded as an intrinsic property of thin PBCO layers.

Similar behavior of sandwich-type junctions with a PBCO barrier has been confirmed by several research groups,[3–5] indicating that the phenomenon occurring in the junctions is reproducible, at least in a qualitative manner. Furthermore, Suzuki *et al.* confirmed a long correlation length of vortices along the *a*-axis direction of YBCO across an *a,b*-axis-oriented PBCO barrier up to 48 nm thickness in their transport measurements of YBCO/PBCO superlattices.[6]

Another puzzling aspect of Josephson junctions with a PBCO barrier is that the junction characteristics seem to depend on the junction geometry. Ramp-edge junctions based on *c*-axis-oriented YBCO films have been reported to exhibit I_cR_n product values almost one order of magnitude larger than those of sandwich-type junctions.[7–9] Direct tunneling and resonant tunneling through localized levels with long localization length have been discussed as a possible mechanism of Josephson coupling in ramp-edge junctions.[7–12] Such localized levels are believed to be associated with the CuO chain in PBCO, for which a unique electronic structure has been predicted theoretically[13] and confirmed experimentally.[14,15] The tunneling model, however, does not give a satisfactory explanation for the dirty SNS behavior observed in sandwich-type junctions.[2]

Recently, Lee *et al.* have demonstrated evidence of metallic conduction along the CuO chain in PBCO up to the millimeter scale at low temperatures in their transport experiments.[16] Although the existence of such a long metallic conduction path is in accordance with proximity coupling in YBCO/PBCO/YBCO junctions, it is contrary to the general understanding that any disorder in a one-dimensional metal entails a localization of electronic states. Further investigation of the current transport and electronic states in PBCO is clearly necessary to clarify the possible mechanism of Josephson coupling in YBCO/PBCO/YBCO junctions.

This paper presents experimental data on current transport in YBCO/PBCO/YBCO sandwich-type junctions in which *b*-axis orientation predominates in the barrier layer, and discusses a possible junction model which can account for the overall features of the observed electrical properties.

II. JUNCTION FABRICATION

YBCO/PBCO/YBCO trilayer films were grown on $SrTiO_3(100)$ substrates by the multitarget sputtering system equipped with Y, Pr, Cu, and BaCu alloy targets.[17] The power supplied to individual targets was controlled precisely to maintain the film composition at the stoichiometric value with a deviation of less than 3%. The substrates were fixed on a substrate holder rotating at a speed of 60 rpm, which guaranteed the homogeneity of the film composition within wafers as well as between wafers. The substrates were placed so as not to pass directly above the targets in order to prevent resputtering by O^- ions and secondary electrons. A 50% O_2-containing Ar/O_2 gas was introduced into the chamber at a pressure of 1.2 Pa, and the substrate temperature was fixed

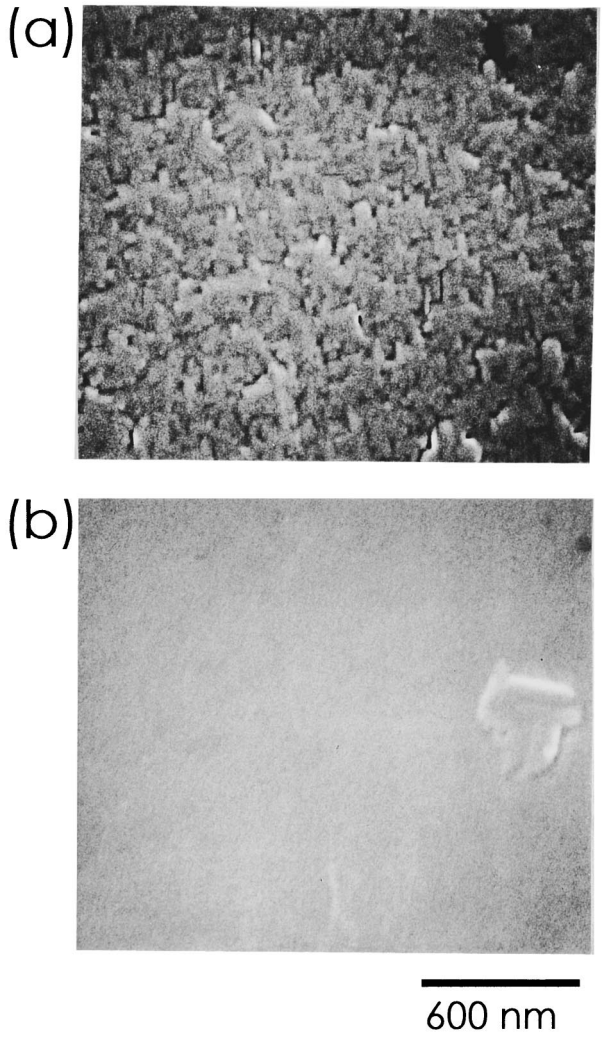

FIG. 1. High-resolution SEM pictures of YBCO/PBCO/YBCO trilayer film surfaces prepared directly on substrate (a) and on a cubic-PrBaCuO buffer layer (b).

at 620 °C throughout the present experiment.

Two types of trilayer films were prepared. In the first type, films were grown directly onto $SrTiO_3$ substrates. Although x-ray-diffraction analysis confirmed that the YBCO layers in these trilayer films exhibited a preferential *a*-axis-oriented growth, a small number of *c*-axis-oriented grains with an irregular shape resembling pyramids were observed in the vicinity of the interface between YBCO films and the substrates by cross-sectional transmission electron microscopy (TEM). Such *c*-axis-oriented grains at the interface affected the surface morphology of *a*-axis-oriented trilayer films, as seen in the scanning electron microscopy (SEM) picture in Fig. 1(a). In the second type, trilayer films were prepared on a thin buffer layer made up of PrBaCuO with a simple perovskite structure having cubic symmetry.[17] This cubic-phase PrBaCuO grew selectively on the $SrTiO_3(100)$ surface at a substrate temperature of 620 °C under relatively higher growth rate conditions. We believe that the cubic phase resulted from the complete mixing of Pr and Ba atoms in the layered perovskite structure and that the chemical formula of the cubic phase film should be described as $(Pr_{1/3}Ba_{2/3})\,CuO_y$. Insertion of the buffer layer improved the surface morphology of the trilayer films significantly, as shown in Fig. 1(b). This improvement in surface morphology was ascribed to the elimination of *c*-axis-oriented grains at the initial stage of film growth.

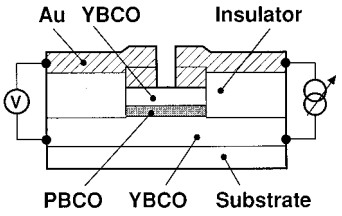

FIG. 2. Schematic representation of junction structure.

Careful x-ray-diffraction measurement revealed that the diffraction from the barrier PBCO in the trilayer films on the buffer layer appeared at the shoulder on the lower angle side of $SrTiO_3(n00)$ diffraction peaks, indicating that the PBCO barrier layer grows with a lattice constant that is slightly longer than $SrTiO_3$. The lattice constant of the PBCO barrier layer along the thickness direction was calculated to be 3.922 Å from the diffraction peaks at high angles. This value corresponds to the *b*-axis length of PBCO in an oxygen deficient condition.[18] We could not observe any diffraction from the barrier PBCO layer on the higher angle side of the $SrTiO_3(n00)$ diffraction peaks. From these results, we concluded that the PBCO layer on *a*-axis-oriented YBCO grew predominantly with *b*-axis orientation, i.e., with the CuO chains normal to the junction surface, which is reasonable from the viewpoint of lattice matching between these two materials. In contrast, we could not observe any diffraction peaks corresponding to PBCO barrier layers separately from those of $SrTiO_3$ for trilayers prepared directly on substrates. This implies that the PBCO layers in unbuffered trilayers grow closer to the tetragonal phase than those in trilayers on a cubic-PBCO buffer.

Both types of trilayer films were utilized for junction experiments to investigate the difference in junction characteristics originating from the difference in the morphology of films as well as in the quality of PBCO barrier layers. Trilayer junctions with the PBCO barrier layer ranging from 10 to 100 nm were fabricated using standard photolithography and the Ar ion milling process. Figure 2 shows a schematic representation of fabricated junctions. The details of the fabrication process have been described elsewhere.[2] The junction dimensions were varied from 5×5 μm^2 to 100×100 μm^2 within a wafer. We fabricated junctions from 18 unbuffered trilayer films as well as from 9 buffered films. From among the large number of junctions, only those exhibiting either clear Josephson characteristics without any excess current or simple resistive properties at low temperatures were selected for detailed investigations, as described in the following section.

III. CURRENT TRANSPORT AT LOW TEMPERATURES

Nearly ideal Josephson characteristics were observed only for unbuffered junctions with a PBCO barrier layer ranging from 20 to 100 nm on seven different wafers. A reasonable scaling of the Josephson current and the junction resistance with junction areas were confirmed for the junctions on the

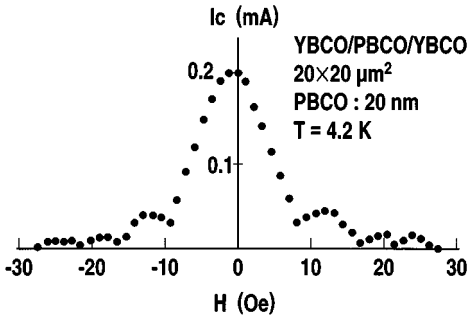

FIG. 3. Magnetic field dependence of the critical current in a YBCO/PBCO/YBCO Josephson junction with a 20-nm-thick barrier layer.

same wafer. Figure 3 shows an example of the magnetic diffraction pattern of the critical current observed for a Josephson junction with a 20-nm-thick barrier. Although the diffraction pattern deviates slightly from an ideal Fraunhofer pattern probably due to the junction size effect,[29] the critical current is periodically suppressed to zero at large magnetic fields. This indicates that the superconducting current flowing in this junction is entirely due to the Josephson effect and that no current paths in which superconductive coupling is stronger than Josephson coupling are formed between two YBCO electrodes. All the junctions with a 10-nm-thick PBCO barrier exhibited superconducting current which did not show any response to the applied magnetic field, indicating that the junction characteristics were governed by vortex flow. The remaining unbuffered junctions except those described above exhibited a mixture of vortex flow and Josephson characteristics. The junctions with any superconducting current insensitive to the applied magnetic field were excluded from our analysis.

In contrast, most of the junctions on a cubic-PBCO buffer with a PBCO barrier layer thicker than 20 nm showed either resistive properties, with a pronounced nonlinear behavior in their current-voltage characteristics at low temperatures, or vortex flow characteristics, depending on the junction area. We selected resistive junctions for which a scaling behavior in junction resistance with the junction areas was confirmed in the same wafer for detailed investigations. One exception to the resistive behavior was found in a junction with a 20-nm-thick barrier for which a Josephson current considerably smaller than that obtained in unbuffered junctions was observed. Some junctions with a 10-nm-thick barrier on a buffer showed partial modulation of the critical current up to 65% by the applied magnetic field. These results indicate that the range of PBCO barrier thickness in which the Josephson effect is observed shifts to the thinner direction for junctions with a buffer layer. The most probable reason for this tendency is the difference in surface morphology between the two types of junctions. In other words, Josephson coupling in unbuffered junctions with a thick PBCO barrier layer is thought to occur selectively in microscopically distributed thin PBCO barrier regions in the inhomogeneous junction structures. It should be, however, mentioned here that the magnitude of a superconducting current insensitive to the applied magnetic field which was often observed for both types of junctions with a PBCO barrier layer thicker than 20 nm, especially for junctions with large areas, did not show a

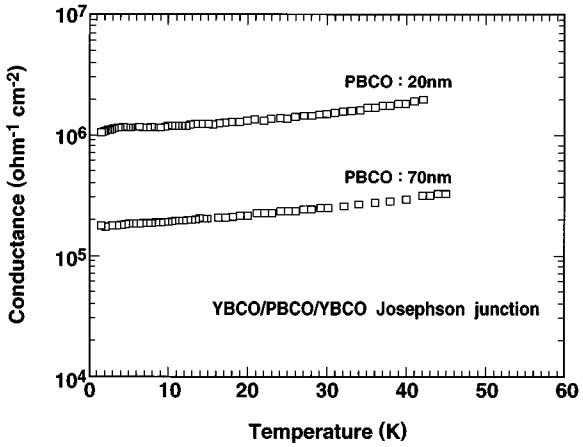

FIG. 4. Temperature dependence of zero-voltage conductance for YBCO/PBCO/YBCO Josephson junctions.

distinct correlation with the morphology of the trilayer films. This implies that the current path for this type of superconducting current, for which simple microshorts between two YBCO electrodes are the most probable origin, is essentially different from that for Josephson current.

In order to clarify the origin of the difference in electrical properties between Josephson junctions and resistive junctions without Josephson characteristics, we measured the temperature and voltage dependence of junction conductance precisely. Figure 4 shows the temperature dependence of zero-voltage conductance observed for trilayer junctions with Josephson characteristics. The junction conductance increased slowly with increasing temperature. Such behavior is common to all the Josephson junctions that we have examined so far, including those not shown in Fig. 4. In contrast, the conductance of junctions with resistive properties exhibited a more complex temperature dependence as shown in Fig. 5. The junction conductance showed a weak temperature dependence similar to that in Josephson junctions at low temperatures, but increased rapidly above 10–20 K, approaching the value in Josephson junctions with a comparable barrier layer thickness. A reasonable explanation for these behaviors of junction conductance is that two conduc-

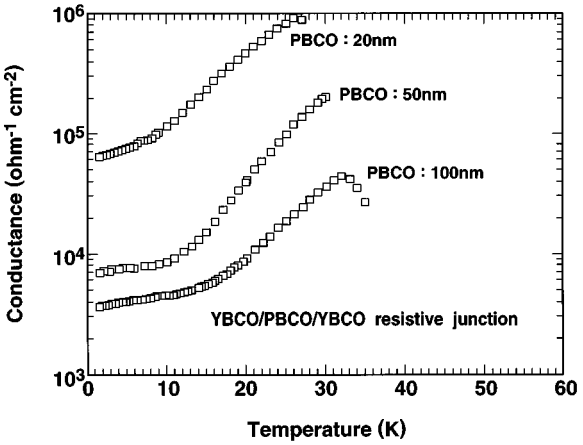

FIG. 5. Temperature dependence of zero-voltage conductance for YBCO/PBCO/YBCO resistive junctions without any evidence of Josephson effect.

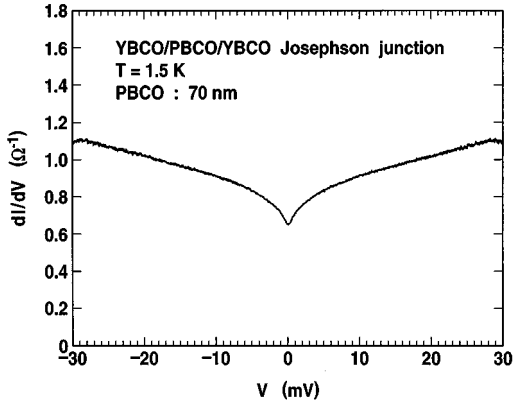

FIG. 6. Zero-bias anomaly in the dI/dV profile at 1.5 K of a YBCO/PBCO/YBCO Josephson junction with a 70-nm-thick barrier.

tion paths exist in parallel within both types of junctions. One path is highly conductive, with weak temperature dependence, and is probably responsible for Josephson coupling, while the other is insulative. Depending on which of these paths is dominant, the apparent junction characteristics are thought to become either Josephson-like or resistive. The behavior of trilayer junctions shown in Figs. 4 and 5 suggests that the effective area of the highly conductive path within the junctions with a given PBCO barrier layer thickness becomes small with the improvement in surface morphology. This indicates that the critical thickness of the PBCO barrier below which the Josephson coupling occurs is far less than the nominal barrier layer thickness in our unbuffered junctions.

Both the Josephson and resistive junctions exhibited a zero-bias anomaly in their differential conductance $G=dI/dV$ versus voltage profiles at low temperatures. This indicates that regardless of the large difference in absolute conductance values between the Josephson and resistive junctions, the same transport mechanism governs the current conduction in these junctions at low temperatures. Figure 6 shows the dI/dV profile of a Josephson junction with a nominally 70-nm-thick PBCO barrier at 1.5 K under a weak magnetic field which suppresses the Josephson current. A symmetrical dip with its minimum at zero voltage is clearly seen. A similar anomaly in dI/dV profile was also observed for resistive junctions, as shown in Fig. 7 with its tempera-

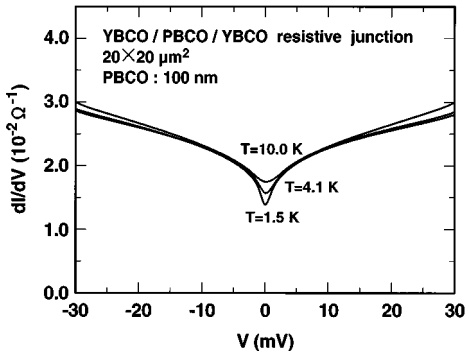

FIG. 7. Temperature dependence of the dI/dV profile of a YBCO/PBCO/YBCO resistive junction with a 100-nm-thick barrier.

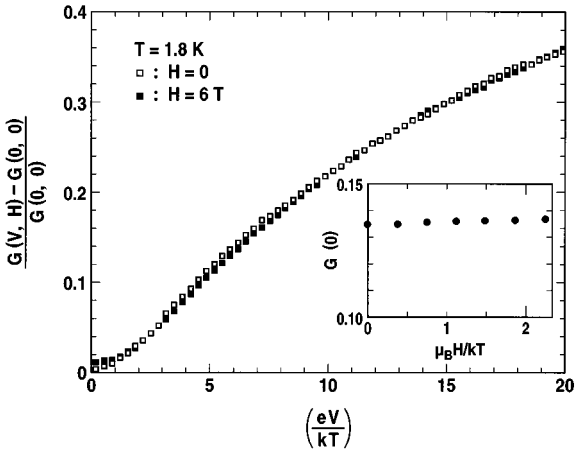

FIG. 8. Voltage dependences of normalized differential conductance at 1.8 K relative to the value at zero voltage in zero magnetic field (open squares) and in a magnetic field of 6 T (solid squares) for a YBCO/PBCO/YBCO junction with a 100-nm-thick barrier. Inset shows the magnetic field dependence of zero-voltage conductance values.

ture dependence. The dip appeared below 10–20 K and deepened with decreasing temperature. The zero-voltage conductance value extrapolated to 0 K using the observed temperature dependence seems to remain at a finite value, as discussed later in this paper.

The magnetic field effect on the conductance dip is depicted in Fig. 8, where differential conductance values at 1.8 K normalized by the zero-voltage conductance in zero magnetic field were plotted against voltages scaled by temperature for applied fields of 0 and 6 T. The inset in the figure is the magnetic field dependence of the zero-voltage conductance $G(0)$. It is apparent that the magnetic field under the present experiment conditions has negligible effects on the conductance dip. This observation was independent of the direction of the applied magnetic field. Although our experimental conditions were not sufficient to detect Zeeman splitting of two spin states of single electrons, the negligibly small magnetic field dependence of the conductance dip is in contrast with the behavior of conductance peaks in Pb/YBCO (Ref. 20) and Ag/YBCO (Ref. 21) junctions, for which an anomalously strong effect of magnetic field was observed under similar conditions.

Conductance dips similar to those shown in Figs. 6 and 7 have been observed before for Pb/YBCO (Ref. 22) and Pb/Au-Ag/PBCO/YBCO (Ref. 23) junctions, as well as in tunneling experiments for nonsuperconductive BiSrCuO.[24] One possible explanation for this type of anomaly is a quantum correction of the density of states at the Fermi energy due to electron-electron interaction in disordered metals containing a large amount of impurities.[25] The quantum correction in the density of states in disordered metals at temperature T can be described by the following equations, with the dimensionality of the system taken as a parameter:

$$N(\varepsilon)-N(0)=a_d\frac{\lambda(k_BT)^{d/2-1}}{(\hbar D)^{d/2}}F_d\left(\frac{\varepsilon}{k_BT}\right), \qquad (1)$$

with

$$F_d(x)=(\cosh x-1)\int_0^\infty \frac{dy}{2y^{2-d/2}}\,\frac{\sinh y}{(1+\cosh y)(\cosh y+\cosh x)}, \tag{2}$$

where $N(\varepsilon)$ represents the density of states at energy ε, d is the dimension of the system, a_d is a constant depending on d, and λ and D denote the electron-electron interaction constant and the diffusion constant, respectively, in disordered metals. If our junctions contain such disordered metal regions adjacent to a tunneling barrier, an anomaly in dI/dV profile reflecting the quantum correction of the density of states would be expected to appear. In the simplest case that the junction has a normal metal–insulator–disordered metal structure and λ is assumed to be independent of energy and temperature, the theoretical dI/dV profile, which is convenient for comparison with experimental results, is approximately given by the following formula:[26]

$$\frac{G(V,T)-G(0,T)}{G(0,T)}=\frac{1}{N_0}\frac{A_d(T)}{4k_BT}\int_{-\infty}^{\infty}F_d\left(\frac{\varepsilon}{k_BT}\right)\left(\frac{1}{\cosh^2\left(\frac{\varepsilon-eV}{2k_BT}\right)}-\frac{1}{\cosh^2\left(\frac{\varepsilon}{2k_BT}\right)}\right)d\varepsilon, \tag{3}$$

with

$$A_d(T)=a_d\frac{\lambda T^{d/2-1}}{(\hbar D)^{d/2}}, \tag{4}$$

where N_0 is the unperturbed density of states of the system. The numerical integration of Eq. (3) is straightforward. We have performed the integration and compared the results with experimentally observed dI/dV profiles.

One example of such a comparison is shown in Fig. 9, where theoretical profiles calculated with the dimensionality of the system as a parameter are plotted together with an experimental result as a function of the square root of the voltage. In spite of the highly simplified model that we used, the theoretical calculation for a three-dimensional disordered metal system showed good agreement with the experimentally obtained profile in the low-voltage region ($eV/kT<25$). However, the experimental profile exhibited a significant deviation from the theoretically predicted square root law at high voltages. Modification of the theoretical model to a disordered metal–insulator–disordered metal structure could not resolve the discrepancy. One possible explanation for the discrepancy may be that Eq. (3) is valid only under the assumption that $\Delta G/G_0 \ll 1$, where ΔG denotes the change in tunneling conductance due to the quantum correction of the density of states and G_0 is the unperturbed tunneling conductance. Although this is true in principle, experimental investigations on disordered aluminum indicate that Eq. (3) gives satisfactory results, even when $\Delta G/G_0 \sim 1$.[26] This seems to refute this possibility.

A similar discrepancy between experimental results and theoretical calculations was also found for the temperature dependence of zero-voltage conductance, as shown in Fig. 10. The experimental data approximately fit the square root function of temperature, which is expected for normal metal–insulator–disordered metal junctions in three dimensions. However, calculations for three-dimensional systems with the same parameters used to fit the dI/dV profile in Fig. 9 showed an increasing discrepancy with an increase in temperature. The discrepancy between theory and experiment seen in Figs. 9 and 10 seems to disappear when one assumes that the actual system has a lower dimensionality, say 2.5, or contains a spatial distribution of three-dimensional and two-dimensional regions. We should, however, be careful to treat the quantum correction of the density of states in low-dimensional systems. The assumption that λ is independent of energy and temperature, which we have used in our analy-

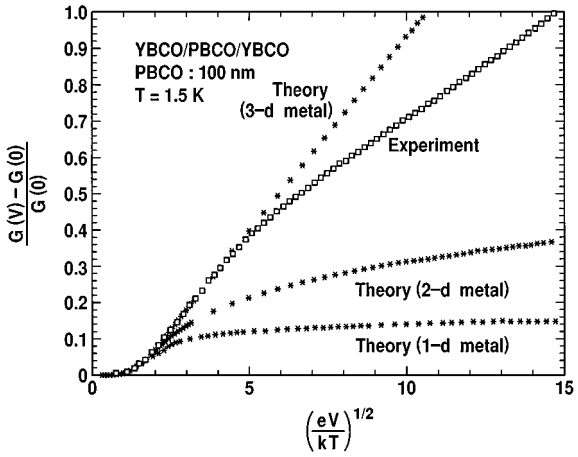

FIG. 9. Comparison between an experimental dI/dV profile and theoretical calculations based on a normal metal–insulator–disordered metal tunnel junction model in various dimensions.

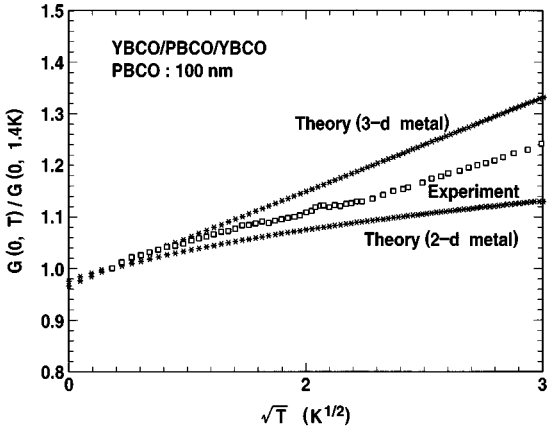

FIG. 10. Plot of zero-voltage conductance as a function of square root of temperature. Open squares show experimental data and asterisks represent the results of calculation with the same parameters as used to fit the dI/dV profile in Fig. 9.

sis, is not justified in cases of low dimensionality.[25] The proper inclusion of the temperature and energy dependence of λ complicates the functional expression of the correction to the density of states in low-dimensionality systems, which makes it difficult to compare experimental results with theoretical calculations. This difficulty makes it impossible for us to discuss further in the present paper whether our junctions really contain disordered metal regions in low dimensions.

Although ambiguity remains regarding the dimensionality of the system, the results shown in Figs. 9 and 10 strongly suggest that the behavior of junction conductance at low temperatures is governed by tunneling through an insulative barrier which lies adjacent to a disordered metal region. We can probably rule out the possibility of resonant tunneling through a localized level with a large on-site Coulomb repulsion, for which a strong magnetic field effect on the zero-voltage conductance has been predicted by theory[27] and confirmed by experiment.[28] The remaining problem is to ascertain which part within the junction serves as a tunneling barrier. Although we do not have definite evidence at present, it seems natural to think that a locally thin PBCO barrier layer acts as the tunneling barrier. If this is actually the case, the disordered metallic region can be thought to be formed within the YBCO layer in close vicinity to the tunneling barrier. It is reasonable to think that superconductivity in the disordered metal region will be considerably suppressed. However, we can also expect the proximity effect due to the underlying or overlying superconductive YBCO electrode in this region. This model is consistent with the fact that dirty metallic weak-link behavior has been observed in our trilayer junctions.[2]

The origin of the formation of a disordered metal region is not clear at present. Interdiffusion of Y and Pr atoms, strain at the YBCO-PBCO interface, and hybridization of the wave function in YBCO with localized states in PBCO are the possible candidates. In any event, we believe that the disordered metallic behavior appears in the vicinity of metal-insulator transition in oxide superconductors. A similar disordered metallic phase without superconductivity has been observed for $La_{1.85}Sr_{0.15}CuO_4$ with impurities substituted for Cu.[29]

IV. HOPPING CONDUCTION AT HIGH TEMPERATURES

The steep increase in the junction conductance at high temperatures observed for the resistive junctions is definitely out of the realm of the tunneling mechanism discussed in the preceding section, and indicates the opening of other conduction channels within the junctions. The data shown in Fig. 5 strongly suggests that a hopping mechanism governs the current transport in these additional channels. An important question with regard to this hopping conduction is whether the variable range hopping (VRH) process usually seen in bulk PBCO (Ref. 30) still governs the current conduction in thin PBCO barrier layers in our junctions. It is recognized that when the thickness of an insulator film with localized states approaches the characteristic hopping distance of VRH, the conductivity of the film is governed by sequential hopping of electrons through specific paths connecting the localized states with the smallest impedance in the forward direction.[31] This effect can be detected as a decrease in apparent characteristic temperature T_0 of VRH with decreasing film thickness. Further reduction in film thickness makes the hopping transport through two or three localized levels dominant at low temperatures, which gives rise to power-law nonlinearities of the current-voltage characteristic as well as of the temperature dependence of conductance.[32]

In order to elucidate whether these size effects appear in our junctions, we have compared the experimental temperature dependence of junction conductance with a model in which a VRH path is assumed to exist in parallel with the tunneling path described in the preceding section. We used the form of VRH conductivity for a three-dimensional system in our analysis:

$$\sigma(T)=\sigma_0\exp(-(T_0/T)^{1/4}), \tag{5}$$

where

$$T_0=\beta\alpha^3/k_B\nu, \tag{6}$$

and ν is the density of localized states at the Fermi level, $1/\alpha$ is the decay length of localized states, and β is a numerical coefficient depending on the choice of models.

Figure 11 shows two examples of such comparison for junctions with thick (100-nm) and thin (20-nm) PBCO barrier layers, where the ordinate represents the conductivity σ of the PBCO barrier which was obtained by normalizing the junction conductance values with the junction area and nominal barrier layer thickness. Excellent agreement is observed between the experimental and the calculated results in both cases. In contrast, junction models based on a current path through a small number of localized levels have not shown satisfactory agreement with experiments, even for junctions with a 20-nm-thick barrier layer. This indicates that hopping conduction through a few localized states does not play a significant role in the current transport in our YBCO/PBCO/YBCO junctions, at least above 10 K. A size effect on hopping conduction, however, has been observed in the thickness dependence of T_0, as shown in Table I. The value of T_0 for a 100-nm PBCO barrier was 4×10^6 K, which is large relative to that of fully oxidized PBCO and is comparable to the values that have been reported for bulk PBCO with slight Ga doping.[33] This suggest that the PBCO barrier layers contain some oxygen atom defects, probably in the CuO chain structures, which may correspond to the short b-axis length observed for the barrier layers. T_0 values remained almost the same for junctions with a 50-nm-thick barrier, but decreased significantly for 20-nm barrier junctions. This implies that a crossover from VRH to sequential hopping along specific paths connecting the localized states with the smallest impedance in the forward direction sets in between 20 and 50 nm in our junctions. From the experimental finding that a significant decrease in T_0 occurs in 20-nm-thick barrier junctions without evidence of electron hopping through a small number of localized states, we can probably conclude that the PBCO layer thickness is comparable with the characteristic hopping distance of VRH in this material, but that it is sufficiently thick compared to the decay length of the wave function at the localized states.

The decay length of localized state $(1/\alpha)$ can be evaluated, at least in principle, from the electric field dependence

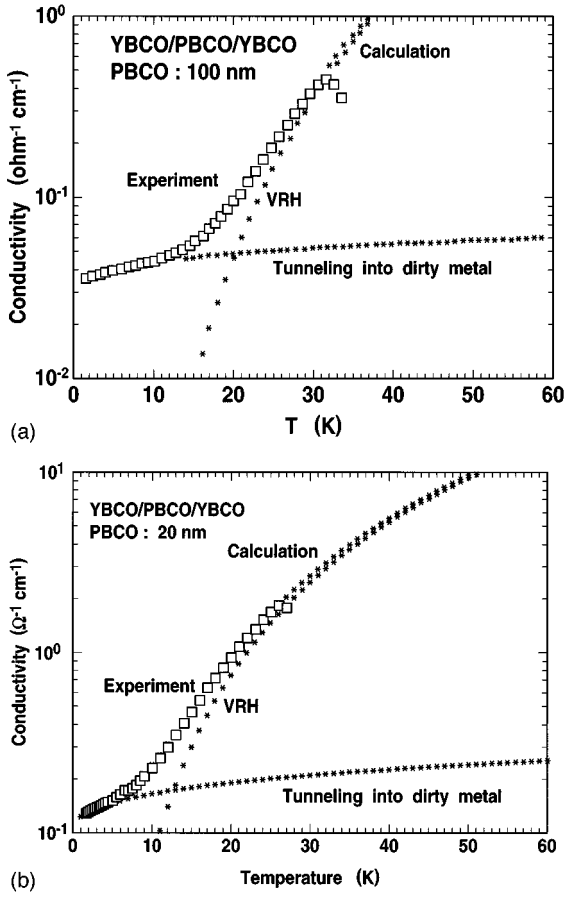

FIG. 11. Theoretical fit of experimental temperature dependences of conductivity of PBCO barrier layers of 100-nm thickness (a) and of 20-nm thickness (b) using a parallel connection model with tunneling and variable range hopping paths.

of VRH conductivity. Apsley and Hughes have given an analytical formula to describe VRH transport at finite electric field F as Eqs. (7) and (8),[34]

$$\sigma(F,T)\approx\sigma_0\exp\left(-\left(\frac{T_0}{T}\right)^{1/4}\left(\frac{2}{P+Q}\right)^{1/4}\right), \tag{7}$$

with

$$P=\frac{1+f/2}{(1+f)^2},\quad Q=\frac{3f}{2}+1,\quad f=\frac{eF}{2\alpha k_B T}. \tag{8}$$

This formula has previously been applied by Kabasawa *et al.* to the analysis of the VRH process in planar-type junctions

TABLE I. Fitting parameters σ_0 and T_0 for hopping conduction in PBCO barrier layers.

PBCO (nm)	σ_0 (Ω^{-1}cm^{-1})	T_0 (K)
100	7.2×10^7	4.0×10^6
50	1.5×10^6	1.1×10^6
	7.5×10^7	3.2×10^6
20	1.7×10^5	4.6×10^5
	3.8×10^4	2.6×10^5

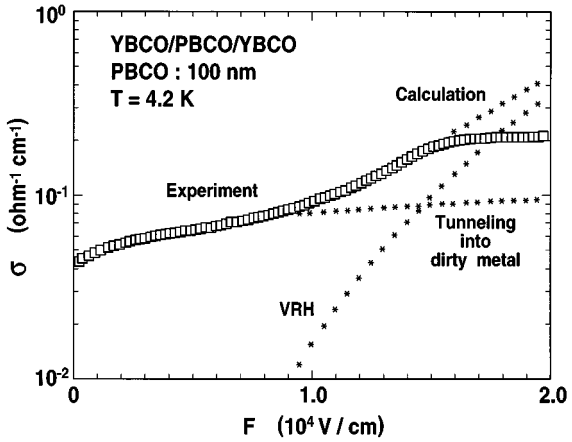

FIG. 12. Electric field dependence of conductivity of a 100-nm-thick PBCO barrier layer at 4.2 K and theoretical fit using a parallel connection model with tunneling and variable range hopping paths.

with a PBCO barrier, with the assumption that the VRH transport in their junction is in two dimensions.[35] We have carried out a similar analysis of our junction characteristics by assuming a three-dimensional VRH process. Figure 12 shows the experimental electric field dependence of conductivity for a 100-nm-thick barrier junction at 4.2 K together with a theoretical fit by a parallel conduction model with VRH and tunneling conduction paths. This theoretical fit gave a value of 3.2 nm for $1/\alpha$. Similarly good agreement between experimental results and the calculation using a $1/\alpha$ value around 3 nm was confirmed for all the junctions with a PBCO barrier ranging from 20 to 100 nm. The density of localized states calculated from T_0 and $1/\alpha$ values using the formula given by Apsley and Hughes was 5.5×10^{17} eV^{-1}cm^{-3} to 3×10^{18} eV^{-1} cm^{-3} for junctions with 100-nm-thick and 50-nm-thick barrier layers.

Although the good agreement between theory and experiment shown in Fig. 12 is impressive, we should probably be cautious in treating the large $1/\alpha$ value as real in our PBCO barrier layers. It is noted that the power dissipation in junctions at high bias voltages exceeds the cooling ability of liquid helium. The dissipated power density of the junction in Fig. 12 at an electric field of 1×10^4 V/cm amounts to 100 W/cm^2, which is thought to be sufficient to give rise to an appreciable increase in junction temperature. It is highly probable that this local heating effect is responsible for the apparent electric field dependence of σ in Fig. 12. Since we do not have any means to determine the actual temperature of junctions, all we can derive from Fig. 12 is that $1/\alpha$ in our PBCO barrier layer is at least smaller than 3 nm. Considering the fact that 10 to 20-nm-thick amorphous silicon films with localized levels with $1/\alpha=0.7$ nm exhibited clear evidence of hopping conduction through a few localized states,[36] the $1/\alpha$ value far smaller than 3 nm seems to be consistent with the result that our 20-nm-thick barrier junction showed no evidence of such a conduction process.

Finally, we would like to compare the above experimental data with other reports on ramp-edge-type junctions and planar-type junctions. Based on the transport measurements for planar-type junctions with a PBCO barrier, Kabasawa *et al.* derived the $1/\alpha$ value in PBCO to be 8.5 nm.[35] This value does not seem to be affected by local heating. Simi-

larly large $1/\alpha$ values have been derived by Satoh *et al.*[9] from the barrier layer thickness dependence of superconducting current and junction conductance observed for ramp-edge junctions with a PBCO barrier, while smaller values between 2 and 4 nm can also be found in other reports by Golubov *et al.*[12] and Sawada *et al.*[8] Furthermore, these authors reported the observation of current transport via a small number of localized states for junctions with a PBCO barrier ranging from 20 to 60 nm at high temperatures as well as at high bias voltages. Although these results give experimental support to the theory of Josephson coupling by resonant tunneling,[11] they are clearly in contrast with our data. A plausible explanation for this discrepancy may be that the electronic states in PBCO are very sensitive to oxygen atom defects in this material. In fact, Suzuki *et al.* demonstrated that the non-VRH transport along CuO chains in PBCO disappeared under oxygen deficient conditions.[6] Both the planar-type junctions and the ramp-edge junctions are based on c-axis-oriented multilayers, for which a higher preparation temperature is required than for a,b-axis-oriented films. It is probable that films prepared at lower temperatures contain more oxygen atom defects in CuO chains, as evidenced by the low critical temperature (<50 K) of our YBCO films and short b-axis length in barrier PBCO. This may result in deepening of the localized levels in PBCO.

V. CONCLUSION

Detailed investigations have been carried out concerning the electrical properties of a,b-axis-oriented YBCO/PBCO/YBCO junctions with a sandwich structure to clarify the transport mechanism and its relevance to Josephson coupling in these junctions. Careful x-ray measurements confirmed that the PBCO barrier layers on a-axis-oriented YBCO films grew predominantly with b-axis orientation including some amount of oxygen deficiency. The elimination of c-axis-oriented grains at the initial stage of film growth by utilizing a buffer layer technique was found to be effective for the improvement in surface morphology of trilayer films.

Two types of junctions with and without the buffer layer were investigated. Josephson coupling thorough a PBCO barrier layer up to 100 nm thickness was observed for junctions without the buffer layer. In contrast, the junctions with better surface morphology on the buffer layer with a PBCO barrier layer thicker than 20 nm showed only resistive properties, with a pronounced nonlinear behavior. This indicates that the presence of Josephson coupling in these junctions at a given PBCO barrier thickness correlated with the surface morphology of trilayer films. In other words, Josephson coupling in unbuffered junctions with a thick PBCO barrier layer is thought to occur selectively in microscopically distributed thin PBCO barrier regions in the inhomogeneous junction structures.

Regardless of the presence or absence of the Josephson effect, most of the junctions exhibited a zero-bias anomaly with a dip in conductance in their dI/dV profiles at low temperatures. This anomaly was attributed to electron tunneling into disordered metal in 2 to 3 dimensions, with a minimum in the density of states due to electron-electron interaction. The tunneling path is inferred to be responsible for Josephson coupling in our junctions. Although superconductivity in the disordered metal region is thought to be considerably suppressed, the proximity effect due to the underlying or overlying superconductive YBCO electrode can be expected in this region. This model is consistent with the fact that the temperature dependence of Josephson current similar to a dirty metallic weak link has been observed in our trilayer junctions.

The complex temperature dependence of junction conductance was reproduced well by a theoretical model in which both tunneling conduction paths and variable range hopping paths were assumed to exist within the PBCO barrier layer. Although we have not obtained any evidence of hopping conduction through a small number of localized states even for junctions with a 20-nm-thick PBCO barrier, a crossover from variable range hopping to sequential hopping along specific paths connecting the localized states with the smallest impedance in the forward direction has been observed to set in at a barrier layer thickness between 20 and 50 nm. These results indicate that a 20-nm-thick PBCO layer is comparable to the characteristic hopping distance of variable range hopping in this material, but is sufficiently thick compared to the decay length of the wave function at the localized states.

Our experimental results are inconsistent with other reports on current transport in ramp-edge-type junctions and planar-type junctions with PBCO barrier layers. This discrepancy may result from the difference in the nature of localized states due to the different preparation conditions between a-axis-oriented and c-axis-oriented films.

ACKNOWLEDGMENT

This work was performed under the management of the R&D Association for Future Electron Devices as a part of the R&D of Basic Technology for Future Industries supported by the New Energy and Industrial Technology Development Organization.

[1] J. B. Barner, C. T. Rogers, A. Inam, R. Ramesh, and S. Bersey, Appl. Phys. Lett. **59**, 742 (1991).

[2] T. Hashimoto, M. Sagoi, Y. Mizutani, J. Yoshida, and K. Mizushima, Appl. Phys. Lett. **60**, 1756 (1992).

[3] A. Fujimaki, H. Terai, Y. Sawada, Y. Takai, and H. Hayakawa (unpublished).

[4] T. Umezawa, D. J. Lew, S. K. Streiffer, and M. R. Beasley, Appl. Phys. Lett. **63**, 3221 (1993).

[5] H. Sato, H. Akoh, and S. Takada, Appl. Phys. Lett. **64**, 1286 (1994).

[6] Y. Suzuki, J.-M. Triscone, C. B. Eom, M. R. Beasley, and T. H. Geballe, Phys. Rev. Lett. **73**, 328 (1994).

[7] Yu. M. Boguslavskij, J. Gao, A. J. H. M. Rijnders, D. Terpstra, G. J. Gerritsma, and H. Rogalla, Physica C **194**, 268 (1992).

[8] Y. Sawada, H. Terai, A. Fujimaki, Y. Takai, and H. Hayakawa, IEEE Trans. Appl. Supercond. **5**, 2099 (1995).

[9] T. Satoh, M. Yu. Kupriyanov, J. S. Tsai, M. Hidaka, and H. Tsuge, IEEE Trans. Appl. Supercond. **5**, 2612 (1995).

[10] J. Halbritter, Phys. Rev. B **46**, 14 861 (1992).

[11] I. A. Devyatov and M. Yu. Kupriyanov, JETP Lett. **59**, 200 (1994).
[12] A. A. Golubov, M. A. J. Verhoeven, I. A. Devyatov, M. Yu. Kupriyanov, G. J. Gerritsma, and H. Rogalla, Physica C **235-240**, 3261 (1994).
[13] R. Fehrenbacher and T. M. Rice, Phys. Rev. Lett. **70**, 3471 (1993).
[14] K. Takenaka, Y. Imanaka, K. Tamasaku, T. Itoh, and S. Uchida, Phys. Rev. B **46**, 5833 (1992).
[15] L. Hoffman, A. A. Manuel, M. Peter, E. Walker, M. Ganthier, A. Shukla, B. Barbiellini, S. Massidda, Gh. Adam, S. Adam, W. N. Hardy, and Ruixing Liang, Phys. Rev. Lett. **71**, 4047 (1993).
[16] M. Lee, Y. Suzuki, and T. H. Geballe, Phys. Rev. B **51**, 15 619 (1995).
[17] T. Nagano, T. Hashimoto, and J. Yoshida, in *Advances in Superconductivity VII*, edited by K. Yamafuji and T. Morishita (Springer-Verlag, Tokyo, 1995), p. 934.
[18] M. E. Lopez-Morales, D. Rios-Jara, J. Taguena, R. Escuders, S. LaPlaca, A. Bezinge, V. Y. Lee, E. M. Engler, and P. Grant, Phys. Rev. B **41**, 6655 (1990).
[19] T. Hashimoto, M. Sagoi, Y. Mizutani, J. Yoshida, and K. Mizushima, IEEE Trans. Appl. Supercond. **3**, 2385 (1993).
[20] J. Lesueur, L. H. Green, W. L. Feldmann, and A. Inam, Physica C **191**, 325 (1992).
[21] S. C. Sanders, S. E. Russek, C. C. Clickner, and J. M. Ekin, Appl. Phys. Lett. **65**, 2232 (1994).
[22] M. Lee, M. Naito, A. Kapitulnik, and M. R. Beasley, Solid State Commun. **70**, 449 (1989).
[23] J. Yoshida and T. Hashimoto, Bull. Electrotech. Lab. **58**, 509 (1994).
[24] A. T. Fiory, S. Martin, R. M. Fleming, L. F. Schneemeyer, and J. V. Waszczak, Phys. Rev. B **41**, 2627 (1990).
[25] B. L. Al'tshuler and A. G. Aronov, in *Electron-Electron Interactions in Disordered Systems*, edited by A. L. Efros and M. Pollak (North-Holland, Amsterdam, 1985), Chap. 1.
[26] M. E. Gershenzon, V. N. Gubankov, and M. I. Falei, Sov. Phys. JETP **63**, 1287 (1986).
[27] L. I. Glazman and K. A. Matveev, JETP Lett. **48**, 445 (1988).
[28] D. Ephron, Y. Xu, and M. R. Beasley, Phys. Rev. Lett. **69**, 3112 (1992).
[29] M. Z. Cieplak, S. Guha, H. Kojima, and P. Lindenfeld, Phys. Rev. B **46**, 5536 (1992).
[30] B. Fisher, G. Koren, J. Genossar, L. Patlagen, and E. L. Gartstein, Physica C **176**, 75 (1991).
[31] M. Pollak and J. J. Hauser, Phys. Rev. Lett. **31**, 1304 (1973).
[32] L. I. Glazman and K. A. Matveev, Sov. Phys. JETP **67**, 1276 (1988).
[33] Y. Xu and W. Guan, Physica C **206**, 59 (1993).
[34] N. Apsley and H. P. Hughes, Philos. Mag. **31**, 1327 (1975).
[35] U. Kabasawa, Y. Tarutani, M. Okamoto, T. Fukazawa, A. Tsukamoto, M. Hiratani, and K. Takagi, Phys. Rev. Lett. **70**, 1700 (1993).
[36] Y. Xu, A. Matsuda, and M. R. Beasley, Phys. Rev. B **42**, 1492 (1990).